



## Feasibility of using calcined *Patinopecten yessoensis* shells for fluoride removal and investigation of the fluoride removal mechanism

Moon-Yeong Choi<sup>a</sup>, Jae-In Lee<sup>b</sup>, Chang-Gu Lee<sup>c</sup>, Seong-Jik Park<sup>a,b,\*</sup>

<sup>a</sup>Department of Bioresources and Rural System Engineering, Hankyong National University, Anseong 17579, Republic of Korea, Fax: +82-31-670-5139; emails: parkseongjik@hknu.ac.kr (S.-J. Park), ahdrmadl123@naver.com (M.-Y. Choi)

<sup>b</sup>Department of Integrated System Engineering, Hankyong National University, Anseong 17579, Republic of Korea, email: sdm02111@naver.com (J.-I. Lee)

<sup>c</sup>Department of Environmental and Safety Engineering, Ajou University, Suwon 16499, Republic of Korea, email: changgu@ajou.ac.kr (C.-G. Lee)

Received 31 March 2021; Accepted 27 June 2021

### ABSTRACT

This study assessed the applicability of seafood waste, *Patinopecten yessoensis* shells (PY), for fluoride removal. PY was modified by calcination to improve its fluoride removal capacity, and 800°C was the optimum calcination temperature its modification as a fluoride adsorbent. Fluoride adsorption by PY-800 was confirmed due to the formation of fluorite (CaF<sub>2</sub>) through X-ray diffraction analysis. The fluorine adsorption to PY-800 reached equilibrium within 2 h at an initial fluoride concentration of 50 mg/L, and a reaction time of 36 h was required to reach equilibrium at 200 mg/L. Both the pseudo-first-order and pseudo-second-order models described the kinetic adsorption data well. In isotherm studies, the fluoride adsorption of PY-800 was best suited to the Langmuir model. The enthalpy change of fluoride adsorption was 45.49 kJ/mol, ranging in the boundary between physical and chemical adsorption. Fluoride adsorption decreased from 113.13 to 86.01 mg/g as the pH increased from 3 to 11. Anions in the solution inhibited fluoride adsorption, and impacted other ions in the following order: chloride < sulfate < carbonate < phosphate. PY-800 has a higher adsorption capacity than other reported adsorbents, with a maximum of 159.62 mg/g. These results show that PY-800 recycled from food waste is highly efficient for fluoride removal.

**Keywords:** *Patinopecten yessoensis* shells; Scallop shell; Fluoride removal; Thermal treatment; Adsorption mechanism

### 1. Introduction

Fluorine is a highly reactive halogen element, usually existing in an ionic form, that is, fluoride in aqueous solution, and it is released to water from igneous and sedimentary rocks in nature [1]. Naturally, fluoride concentrations in groundwater range from trace to 48 mg/L [2], its concentration up to 30 mg/L occurs in the United States of America, Africa and Asia [1]. Wastewater containing dissolved fluorine by industrial activities can significantly

affect the environment and public health. Water with low concentrations of fluoride suppresses germs in the mouth and hardens the teeth, giving teeth an advantage. However, long-term consumption of fluoride-containing water causes chronic dentation and skeletal fluoridation, which turns the teeth brown and weakens the bone [3]. According to the World Health Organization (WHO), the recommended fluoride concentration in drinking water is below 1.5 mg/L [4].

\* Corresponding author.

Scientists have extensively studied low-cost and practical methods to remove fluoride from water and wastewater. Purification methods for water contaminated with fluoride include coagulation, membrane, reverse osmosis, nanofiltration, electrodialysis, and adsorption [5]. Coagulation methods have generally been effective in defluorination, but have failed to bring fluoride to the desired concentration level despite using excessive chemicals [6]. Membrane processes do not require chemical additives, but are relatively expensive to install and operate, and are prone to scaling, fouling, or membrane degradation [7]. Additionally, electrodialysis technology is generally inconvenient because of its high cost during installation and maintenance [6]. Among the methods used for the defluorination of water, adsorption is considered to be adjustable, environmentally friendly, and economical [8].

Al, Ca, and La-based materials were used as adsorbents for fluoride removal because fluoride forms a strong bond with Al, Ca, and La [1]. Various materials originated from natural/modified clay such as kaolinite, bentonite, pyrophyllite [9], dolomite [10], sepiolite [11]; industrial/domestic wastes such as red mud [12], steel slag [13], crushed concrete [14], and eggshells [15]; synthetic materials such as metal oxide [16], nanoparticles [17], and biochar [18] have been applied for fluoride removal. Calcium-based adsorbents have been evaluated to be excellent adsorbents for fluorine removal because their use can avoid the potential health risks of metal leaching [7,19]. Using by-products or wastes as an adsorbent for fluoride removal has advantages in low cost and recycling of resources. Especially bio-originated materials can cause less public concern for water treatment application. However, the major drawback of these adsorbents is their relatively low adsorption capacity [20].

*Patinopecten yessoensis* (PY) scallops are produced along the east coast of Korea and are consumed by many seafood manufacturers and restaurants. A significant amount of scallop shells is discharged into the environment as waste, and recycling of scallop shells as adsorbents for contaminant removal can be attempted. In previous studies [21–23], scallop shells were found to be effective for phosphate removal as they were mainly composed of calcium carbonate. It is expected that a high calcium carbonate content in scallops can also aid in removing fluoride from aqueous solutions. However, only a few studies have attempted to apply scallop shells as adsorbents for fluoride removal [21–23], and to the best of our knowledge, scallop shells were not calcined to enhance their fluoride removal capacity. A systematic study of applying scallops as alternative low-cost adsorbents for removing fluoride from water and wastewater is also required.

In this study, the applicability of PY as an adsorbent to remove fluoride from water and wastewater was assessed, and the simple method of calcination was suggested to improve the fluoride removal capacity of PY. The physical and chemical characteristics of PY calcined at different temperatures were analyzed using several methods, and these data were used to investigate the scientific reasons for the different adsorption capacities of PY depending on the calcination temperature. Kinetic, equilibrium, and thermodynamic adsorption studies were conducted under

batch conditions, and the results were fitted to mathematical models. Other environmental conditions, including the solution pH, the presence of inhibiting anions, and the capacity of the adsorbent were determined through batch tests.

## 2. Materials and methods

### 2.1. Preparation and characterization of pyrolyzed adsorbents

The PY used in the experiment was provided at a restaurant near the campus (Anseong City, Korea), and the experiment was conducted after washing the PY thrice with deionized water and drying at 105°C. The PY particles were produced at a uniform size (425–850 µm) using US standard sieves. PY was calcined to enhance its fluoride adsorption capacity, and calcination was conducted at different temperatures to determine the optimum temperature. Nitrogen gas was injected into a muffle furnace (CRFT 830S, Dongseo Science Co., Ltd., Korea) to create oxygen-free conditions, and heat was applied at a heating rate of 20°C/min for 4 h. The temperatures set for the calcination were 100°C, 300°C, 500°C, 700°C, 800°C, and 900°C, and the abbreviations designated for PY calcined at each temperature were PY-100, PY-300, PY-500, PY-700 PY-800, and PY-900, respectively. After four h heat treatment at the set temperature, the calcined PYs were cooled in the furnace at room temperature.

The calcined PY at various temperatures (0°C–900°C) was characterized using various methods. A field-emission scanning electron microscope (FE-SEM; S-4700, Hitachi, Japan) was used to observe the surface morphology of PY. X-ray fluorescence spectroscopy (XRF; Primus ZSX 4, Rigaku, Japan) was employed to analyze the elemental composition of PY calcined at various temperatures. The mineralogical structures of the different PYs were investigated by analyzing their X-ray diffraction (XRD) patterns (Smartlab, Rigaku, Japan). A thermogravimetric analyzer (TGA; Pyris1, Perkin-Elmer, USA) was used to analyze the mass change according to the temperature of the PY. The specific surface area of samples was determined by interpreting the nitrogen adsorption isotherm data obtained from a surface area analyzer (Autosorb-iQ, Quantachrome Corporation, USA) using Brunauer–Emmett–Teller equation.

### 2.2. Adsorption experiment

Fluoride adsorption by PY calcined at different temperatures was quantified through batch tests, and their capacities were compared. The right amount of adsorbents (0.1 g of each PY), and 30 mL of a 50 mg/L fluoride solution were added to a 50 mL conical tube, and the conical tube was shaken at 25°C and 100 rpm for 24 h in a shaking incubator (SJ-808SF, Sejong Scientific). The solution was filtered after the reaction to separate it from the adsorbents and PY, using filter paper (0.45 µm cellulose acetate, membrane filter, Advantec, Japan). The filtered solution was analyzed by ion chromatography (DX-120, Dionex, USA). The fluoride adsorption amount was calculated by dividing the difference in fluoride concentration before

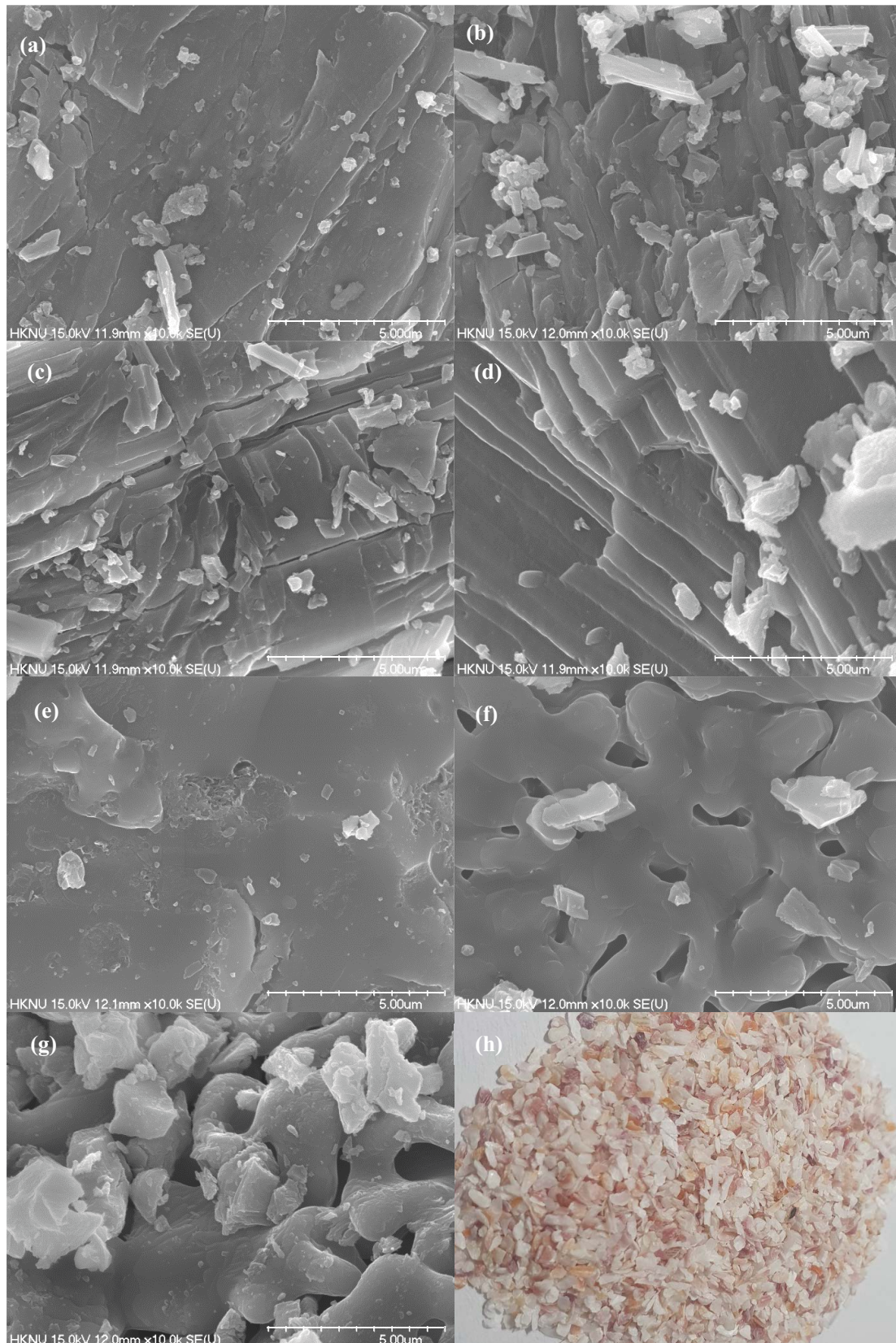


Fig. 1. FE-SEM images of (a) untreated PY (PY-NT) and PY treated at (b) 100°C (PY-100), (c) 300°C (PY-300), (d) 500°C (PY-500), (e) 700°C (PY-700), (f) 800°C (PY-800), and (g) 900°C (PY-900). Operating conditions for FE-SEM images are as: accelerating voltage: 15.0 kV; magnification:  $\times 10,000$ ; scale bar: 5.00  $\mu\text{m}$ . (h) Digital image of nascent and untreated PY.

and after the reaction by the amount of the adsorbent used. All experiments were conducted in triplicate to obtain consistent data. Unless otherwise noted, all experiments were conducted under the aforementioned conditions.

PY calcined at 800°C, which was found to be the optimum temperature, was used for further experiments to investigate the adsorption characteristics of fluoride on PY-800. In a kinetic experiment, the time required to reach PY-800 with fluoride varied from 0.25 to 24 h, and these experiments were conducted under two initial concentrations (50 and 200 mg/L). These concentrations were set to simulate high fluoride concentration in groundwater and industrial wastewater. The experimental data were analyzed using pseudo-first-order (PFO) and pseudo-second-order (PSO) models. In the equilibrium adsorption experiment, the initial fluoride concentration varied (5–1,000 mg/L), and the dosage amount of PY-800 was fixed at 3.33 g/L. The experimental data were plotted as residual fluoride concentration vs. fluoride adsorption by PY-800 and fitted to the Langmuir and Freundlich models. Thermodynamic adsorption experiments were conducted by making fluoride react with PY-800 at three different temperatures (15°C, 25°C, and 35°C). The influence of the solution chemistry, including the pH and inhibiting anions, was also assessed. The pH of the 300 mg/L fluoride solution was adjusted to 3, 5, 7, 9, and 11 using 0.1 M HCl and 0.1 M NaOH. Bicarbonate, sulfate, chloride, and phosphate were prepared by dissolving 0.001 and 0.01 M NaHCO<sub>3</sub>, Na<sub>2</sub>SO<sub>4</sub>, NaCl, and K<sub>2</sub>HPO<sub>4</sub> in a 300 mg/L fluoride solution, respectively. The effect of adsorbent dosage on both the fluoride removal percentage and adsorption amount per unit mass of adsorbents were also quantified by varying the PY-800 dosage from 0.1 to 0.5 g, while the solution volume was fixed at 30 mL of 300 mg/L fluoride solution.

### 3. Results and discussion

#### 3.1. Analysis of the fluoride adsorption capacity and characteristics of pyrolyzed PY

The effect of calcination temperature on the physical and chemical properties of PY was evaluated through various analyses. The surface texture and morphology of PY calcined at different temperatures were observed using

FE-SEM and are shown in Fig. 1. Untreated PY has a non-porous structure, and some of the fragments were observed on the surface of untreated PY, as shown in Fig. 1a. The striped surface with fragments was observed from PY-300 and PY-500, and the surface of PY-700 became smooth owing to the melting of the surface. Pores appeared in the PY-800 and PY-900 samples. The specific surface area of PY was increased from 0.843 to 6.98 m<sup>2</sup>/g as the calcination temperature increase from none treatment to 900°C.

The elemental compositions of PY calcined at different temperatures are presented in Table 1. Untreated and calcined PY mainly consist of Ca and C with minor amounts of S, Na, Mg, and Sr. This is because PY is composed mainly of minerals containing Ca, such as calcite [24]. When the thermal temperature on PY increased, the Ca content increased, but the C content decreased. This result is attributed to the decomposition of CaCO<sub>3</sub> into CaO under thermal treatment, and CO<sub>2</sub> is released from the calcite, leading to a decrease in the C content [25].

The XRD analysis results of untreated and calcined PY are shown in Fig. 2, and their mineral compositions are presented in Table 1. Raw PY (PY-NT) has peaks relevant to calcite (CaCO<sub>3</sub>) and aragonite (CaCO<sub>3</sub>) (Fig. 2a), and aragonite (85.0%) is predominant compared to calcite (14.9%). The peaks of CaO (lime and portlandite) began to appear at a calcination temperature of 700°C, and the CaCO<sub>3</sub> (calcite) content decreased significantly. As the calcination temperature increased to 900°C, the CaO content increased continuously, while that of CaCO<sub>3</sub> decreased. These results can be compared to the TGA data, which show a rapid weight loss above 700°C, as shown in Fig. 3. The weight (%) of PY was decreased from 94.8% to 71.5% as the calcination temperature increase from 700°C to 800°C. Hu et al. [26] reported that the weight loss at 600°C–750°C was caused by the change of CaCO<sub>3</sub> to CaO. This is also consistent with the elemental composition data showing that the C content of PY sharply decreased above 700°C due to the release of CO<sub>2</sub> from CaCO<sub>3</sub>, as described above.

The fluoride adsorption capacity of PY, which was changed by pyrolysis at various calcination temperatures, is shown in Fig. 4. The PY with thermal treatment temperatures from 0°C to 500°C show very low

Table 1  
Elemental and mineral compositions of untreated and calcined PY obtained from X-ray fluorescence spectrometer and X-ray diffraction analysis

Adsorbent	Elemental composition (wt.%) <sup>a</sup>							Mineral composition (%) <sup>b</sup>				
	Ca	C	S	Na	Mg	Sr	Cl	Calcite	Carbon	Aragonite	Portlandite	Lime
PY-NT	67.9	30.2	0.5	0.4	0.4	0.2	–	14.9	0.1	85.0	–	–
PY-100	68.2	30.1	0.4	0.5	0.4	0.2	–	95.0	1.5	3.5	–	–
PY-300	68.9	29.4	0.4	0.4	0.4	0.2	–	97.0	2.5	0.1	–	–
PY-500	68.9	29.0	0.4	0.6	0.4	0.2	0.2	99.0	0.7	0.1	–	–
PY-700	72.5	24.8	1.2	0.6	0.4	0.2	0.2	94.5	–	–	5.2	0.3
PY-800	80.7	17.3	0.4	0.7	0.5	0.3	–	57.5	–	–	40.8	1.7
PY-900	88.6	9.9	0.4	0.2	0.5	0.3	–	–	–	–	94.39	5.61

<sup>a</sup>obtained from X-ray fluorescence spectrometer;

<sup>b</sup>obtained from X-ray diffraction.

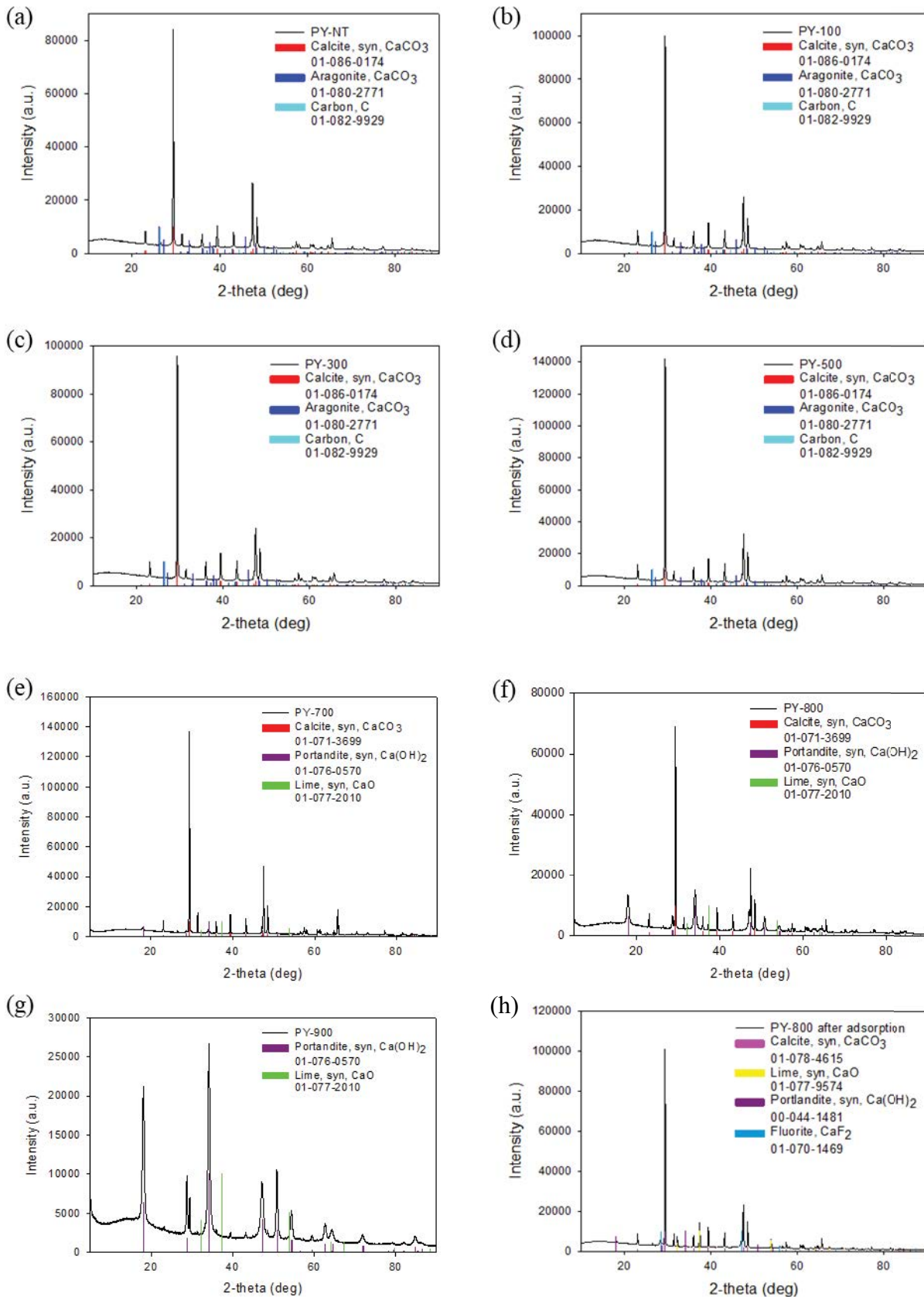


Fig. 2. XRD patterns of (a) PY-NT, (b) PY 100°C, (c) PY 300°C, (d) PY 500°C, (e) PY 700°C, (f) PY 800°C, (g) PY 900°C, and (h) PY-800 after adsorption.

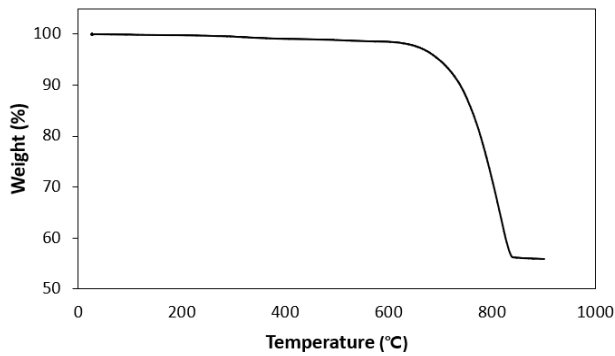


Fig. 3. Weight change of PY as a function of temperature obtained from TGA analysis.

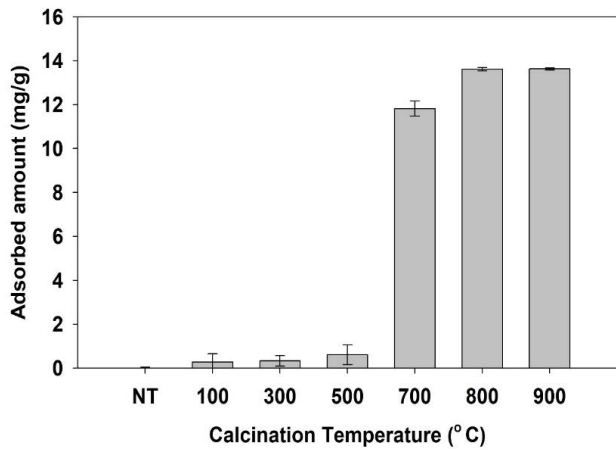


Fig. 4. Effect of the calcination temperature of PY on the fluoride adsorption amount (initial concentration: 50 mg/L; reaction time: 24 h; sorbent dose: 3.33 g/L; reaction temperature: 25°C, pH 7).

fluoride adsorption. However, the adsorption capacity of PY for fluoride increased significantly at 700°C and further increased at 800°C–900°C, wherein their adsorption capacities were similar (14.12 and 14.26 mg/L, respectively). The higher fluoride adsorption capacity of PY-800 compared to that of PY-700 can be explained by the results obtained from the XRD analysis. At higher thermal treatment temperatures, a considerable amount of CaO was formed, which enhanced the solubility of Ca<sup>2+</sup> from the

adsorbents to the solution compared to CaCO<sub>3</sub>. The solubility product constants for CaCO<sub>3</sub> and Ca(OH)<sub>2</sub> were 3.36 × 10<sup>-9</sup> and 5.02 × 10<sup>-6</sup>, which correspond to Ca<sup>2+</sup> solubilities of 5.80 × 10<sup>-5</sup> and 1.08 × 10<sup>-2</sup>, respectively [20]. PY-800 released more Ca<sup>2+</sup> ions that removed more F<sup>-</sup> ions from the solution as a precipitate (CaF<sub>2</sub>), compared to PY-700 [27–29]. In Fig. 2e, fluoride removal via the formation of fluorite (CaF<sub>2</sub>) was revealed by the XRD results for PY-800 after fluoride adsorption. The peaks of CaF<sub>2</sub> were observed in PY-800 after fluoride adsorption, and CaF<sub>2</sub> consisted 13.9% while the contents for CaCO<sub>3</sub>, Ca(OH)<sub>2</sub>, and CaO were 48.0%, 37.0%, and 1.4%, respectively. To obtain an efficient adsorbent for fluoride removal using less energy for calcination, PY-800 was selected as the ideal adsorbent for subsequent experiments and studies.

### 3.2. Kinetic fluoride adsorption results of PY-800

Adsorption kinetics with respect to the reaction time is helpful for understanding the mechanism of fluoride adsorption [30]. The effect of contact time between PY-800 and the fluoride solution on the fluoride removal was investigated by varying the contact time (0.25–120 h) with initial concentrations of 50 and 200 mg/L (Fig. 5). At low concentrations (50 mg/L), the amount of fluoride adsorption on PY-800 increased to 15.39 mg/g within 2 h, and it formed a plateau when it reached 15.66 mg/g after 48 h. At high concentrations (200 mg/L), the fluoride adsorption on PY-800 increased continuously to 59.19 mg/g over 36 h, and the adsorption capacity was constant until even 120 h. Initially, the adsorption area on the surface of PY-800 was empty, so fluoride adsorption was fast, but the adsorption rate slowed when the adsorption site on the surface of PY-800 was filled by adsorbed fluoride at equilibrium.

To verify the adsorption characteristics and the mechanism of fluoride adsorption by PY-800, we analyzed the experimental data using the PFO and PSO models. The parameter values for PFO and PSO are presented in Table 2, where  $q_e$  is the adsorption capacity at equilibrium,  $q_t$  is the adsorption capacity at time  $t$ ,  $k_1$  is the PFO adsorption rate constant, and  $k_2$  is the PSO rate constant.  $R^2$  has a higher value in the PFO model than in the PSO model, indicating that this adsorption model is more suitable for the PFO model. Additionally, the equilibrium adsorption capacities ( $q_e$ ) obtained from PFO are 15.85 and 60.61 mg/g, respectively, which are close to the experimental capacities (15.66 and 59.19 mg/g, respectively). This finding suggests that

Table 2  
Parameters of the PFO and PSO models obtained through model fitting

	Observed $q_e$ (mg/g)	Pseudo-first-order kinetic model parameters $q_t = q_e (1 - \exp(-k_1 t))$			Pseudo-second-order kinetic model parameters $q_t = \frac{k_2 q_e^2 t}{1 + k_2 q_e t}$		
		$q_e$ (mg/g)	$k_1$ (1/h)	$R^2$	$q_e$ (mg/g)	$k_2$ (g/mg/h)	$R^2$
50 mg/L	15.66	15.85	1.833	0.982	16.68	0.178	0.972
200 mg/L	59.19	60.61	0.0791	0.990	70.37	0.0879	0.971

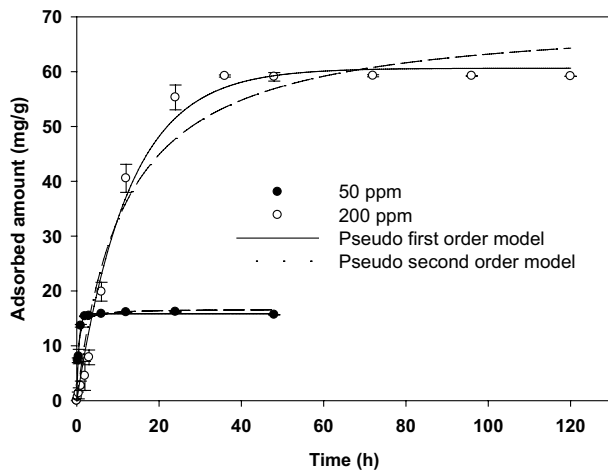


Fig. 5. Relationship between the reaction time and fluoride adsorption amount of PY-800 using PFO and PSO model fit (initial concentration: 50 and 200 mg/L; reaction temperature: 25°C).

Table 3  
Parameters of the Langmuir and Freundlich models obtained through model fitting

Model	Parameters		$R^2$
Langmuir	$Q_m$ (mg/g)	$K_L$ (L/mg)	0.931
	159.62	23.837	
	$q_e = \frac{Q_m K_L C}{1 + K_L C}$		
Freundlich	$K_F$ (L/g)	$1/n$	0.869
	19.434	0.344	
	$q_e = K_F C_e^{1/n}$		

the kinetic adsorption data of this experiment follows the non-linear expression of the PFO model, indicating that the rate-controlling step of fluoride onto PY-800 was primarily governed by physical adsorption [31]. However, as the  $R^2$  value of the PSO model was also high, this adsorption is also known to be affected by chemical adsorption.

### 3.3. Equilibrium adsorption isotherms

Equilibrium adsorption experimental data were analyzed using isothermal models to obtain the maximum adsorption capacity and investigate the adsorption mechanism [32,33]. The equilibrium adsorption study was conducted by varying the initial concentrations from 5 to 1,000 mg/L, and the fluoride adsorption based on equilibrium (or residual) concentrations was plotted with the two model fits shown in Fig. 6. The fluoride adsorption capacity of PY-800 increased with increasing initial fluoride concentrations.

For isotherm studies, the data were analyzed using the Langmuir and Freundlich isotherm models, and the determined parameters are presented in Table 3. In the Langmuir model,  $q_m$  (mg/g) is the maximum fluoride

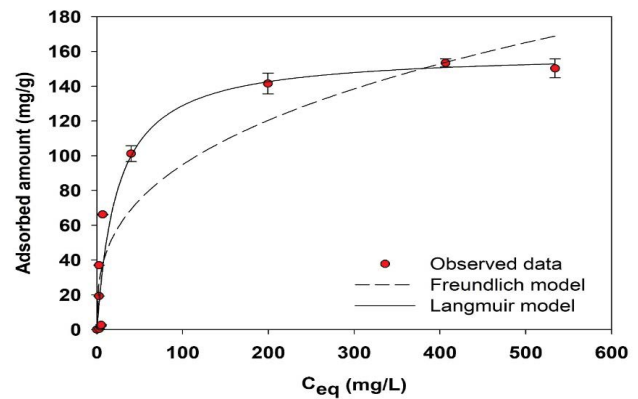


Fig. 6. Relationship between the equilibrium concentration and adsorbed fluoride concentration on PY-800 with Langmuir and Freundlich model fits (adsorbent dose: 3.33 g/L; reaction time: 24 h; reaction temperature: 25°C).

adsorption amount, and  $K_L$  (L/mg) is the Langmuir constant related to the affinity of the binding energy. In the Freundlich model,  $K_F$  is the Freundlich constant, and  $1/n$  is the adsorption strength. The closer the  $R^2$  value is to 1, the better is the isotherm model for adsorption. The  $R^2$  of the Langmuir model was 0.931, which was higher than that of the Freundlich model (0.869). This indicates that the fluoride adsorption of PY-800 is more suitable for the Langmuir model. The fact that the experimental data are explained well by the Langmuir model implies the monolayer coverage of fluoride onto PY-800 and the homogeneous distribution of active sites on the PY-800 surface [34]. The maximum fluoride adsorption amount of PY-800 obtained from the Langmuir model fitting was 159.62 mg/g, which was higher than reported in the literature (Table 4), except for CaO nanoparticles [35]. Compared to nano-sized adsorbents, PY-800 is advantageous owing to its easy synthesis, low cost, and easy separation after adsorption. The  $1/n$  value obtained from the Freundlich model was less than 0.5, indicating substantial binding between fluoride and PY-800 [36].

### 3.4. Thermodynamic adsorption properties

To study the temperature dependence of PY-800 on fluoride adsorption, the reaction temperature was set to 15°C, 25°C, and 35°C. The fluoride adsorptions at 15°C, 25°C, and 35°C were 39.15, 58.32, and 62.85 mg/g, respectively, indicating that the fluoride adsorption capacity of PY-800 increased as the reaction temperature increased. The thermodynamic parameters were obtained from the van't Hoff plot (Fig. 7) using  $\ln(\alpha q_e/C_e) = \Delta S^\circ/R - \Delta H^\circ/RT$  equation [10] and are presented in Table 5. With respect to the parameters obtained, the fluoride adsorption of PY-800 had a positive enthalpy ( $\Delta H^\circ$ ), exhibiting endothermic properties. The value of  $\Delta H^\circ$  of PY-800 is 45.49 kJ/mol, which is slightly less than the heat of chemical adsorption (80–200 kJ/mol), but above the criteria of physical adsorption (2.1–20.9 kJ/mol) [43]. Therefore, fluoride adsorption may proceed at the boundary between chemical and physical adsorption. This result can also

Table 4  
Comparison of the maximum adsorption capacity of fluoride for various adsorbents

Adsorbent	Langmuir adsorption capacity (mg/g)	Reference
Calcite	0.39	[20]
Charcoals contain dispersed aluminum oxide	13.6	[37]
Alum-impregnated activated alumina	40.68	[38]
Aluminum alginate composite	79.22	[39]
Aluminum hydroxide impregnated limestone (AILS)	84.03	[40]
Calcium oxide-modified activated alumina	101.01	[41]
CaO loaded mesoporous Al <sub>2</sub> O <sub>3</sub>	136.99	[42]
CaO nanoparticles	163.3	[35]
Activated <i>Patinopecten yessoensis</i> shell	159.62	This work

Table 5

Thermodynamic parameters of fluoride adsorption to PY-800 ( $\Delta G^\circ$ : change in Gibbs free energy;  $\Delta S^\circ$ : change in entropy;  $\Delta H^\circ$ : change in enthalpy;  $T$ : absolute temperature (K);  $R$ : universal gas constant (8.314 J/mol/K),  $K_c$ : equilibrium constant;  $\alpha$ : amount of adsorbent)

Temperature (°C)	$\Delta H^\circ$ (kJ/mol)	$\Delta S^\circ$ (J/K mol)	$\Delta G^\circ$ (kJ/mol) $\Delta G^\circ = -RT \ln K_c$
15	45.49	147.63	2.96
25			1.48
35			0.005

be confirmed by the results of the kinetic adsorption study in which both the PFO and PSO models described the experimental data well. Positive entropy values ( $\Delta S^\circ$ ) indicate an increase in the degree of disorder at the interface between the solid and solution, and positive free energy values ( $\Delta G^\circ$ ) indicate involuntary reactions under these experimental conditions [44,45].

### 3.5. Chemical effects on fluoride adsorption

The solution pH is considered to be an essential factor for quantifying the fluoride removal efficiency of adsorbents and the mechanism of fluoride adsorption. This is because the pH of the solution affects both the ion species of the target contaminants and the surface charge of the adsorbent [35,46]. The fluoride adsorption by PY-800 at different solution pH values is illustrated in Fig. 8a. The increase of pH from 3 to 11 suppressed the fluoride adsorption on PY-800 from 113.13 to 86.01 mg/g, indicating that the fluoride adsorption was inversely proportional to the solution pH. The decrease in fluoride adsorption under alkaline conditions can be explained by the competition of OH<sup>-</sup> and F<sup>-</sup> for the surface area of the adsorbent or the electrostatic repulsion of F<sup>-</sup> against the negatively charged adsorbent surface [47,48].

Feeding water contains anions other than fluoride, which may affect the adsorption of fluoride. Adsorption studies were conducted with fluoride solutions containing 0.01 and 0.001 M of bicarbonate, sulfate, chloride, and phosphate, respectively. The change in fluoride adsorption due to the presence of anions is shown in Fig. 8b. The effect of chloride on the ability of the sorbent to defluorinate was

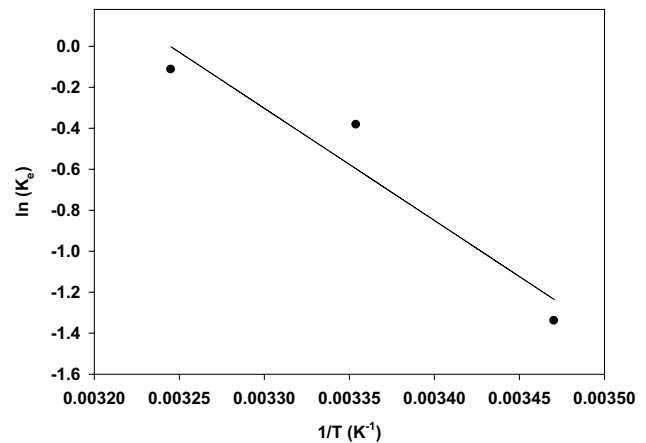


Fig. 7. Van't Hoff plot for fluoride adsorption to PY-800 under different temperatures (15°C–35°C) ( $K_c$ : equilibrium constant;  $T$ : absolute temperature (K); initial fluoride concentration: 300 mg/L; reaction time: 24 h; adsorbent dose: 3.33 g/L).

insignificant. In contrast, ions other than chloride interfered in the removal of fluoride ions from the adsorbent, and the interference increased with the concentration of the ions. The interference is due to the formation of precipitates with Ca<sup>2+</sup>; however, sulfate ions react with Ca<sup>2+</sup> of the adsorbent to produce CaSO<sub>4</sub> with a high solubility, which has less effect on fluoride adsorption [20]. In the presence of 0.01 M of phosphate, the adsorption of fluoride was strongly suppressed from 101.8 to 28.86 mg/g due to the electrostatic interaction and complexation of the adsorbent surface [49].

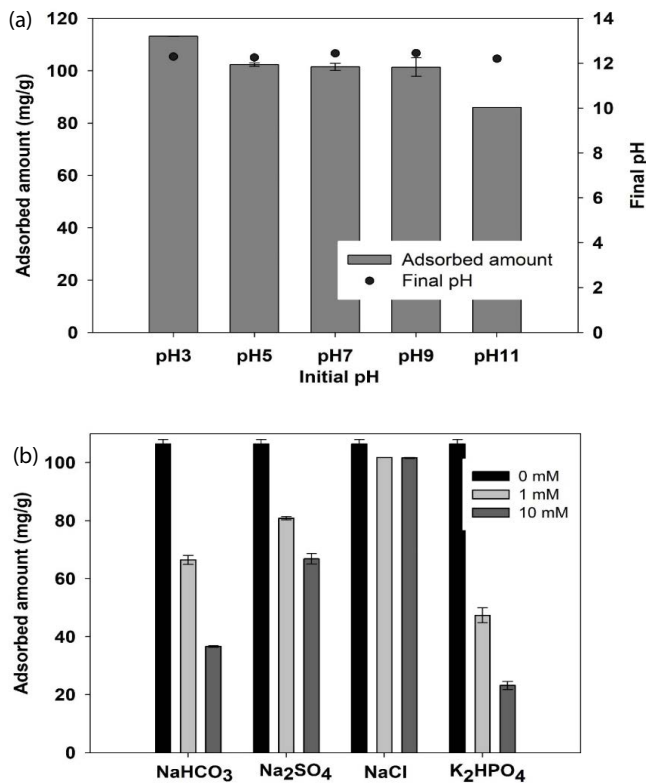


Fig. 8. (a) Effect of pH and (b) coexisting ions on the adsorbed amount of PY-800 (initial fluoride concentration: 300 mg/L; reaction time: 24 h; adsorbent dose: 3.33 g/L; temperature: 25°C).

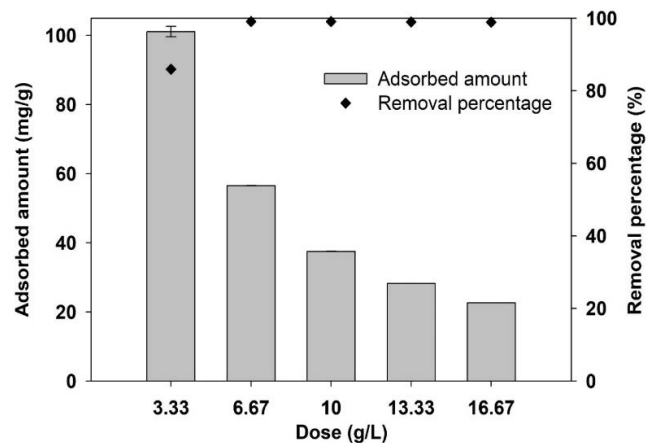


Fig. 9. Effect of adsorbent dosage on the fluoride adsorption capacity and removal percentages (initial fluoride concentration: 300 mg/L; reaction time: 24 h; temperature: 25°C).

### 3.6. Amount of adsorbent dosage for optimal fluorine removal

The effect of the adsorbent dose on fluoride adsorption is shown in Fig. 9. The adsorption amount per unit mass was 101.1 mg/g when the adsorbent capacity was 3.33 g/L. With the increase in the adsorbent dosage, the adsorbent capacity per unit mass decreased continuously (56.54 mg/g at 6.67 g/L, 37.55 mg/g at 10.00 g/L, 38.24 mg/g at 13.33 g/L,

and 22.58 mg/g at 16.67 g/L). The decrease in the adsorption capacity per unit mass of adsorbent can be explained by the fact that the addition of PY-800 provided more adsorbable sites for fluoride, leaving the space not adsorbed by fluoride [39,50]. The removal efficiency was 85.93% when the adsorbent capacity was 3.33 g/L. When the dosage increased to 6.67 g/L, the removal percentage reached 99.1%, and it was maintained above 99% at an adsorbent dosage of over 6.67 g/L. A high removal percentage can be observed compared to other fluoride removal adsorbents such as calcite (12%) [27], activated alumina (69.5%) [27], gas concrete (86%) [35], CaO-loaded mesoporous Al<sub>2</sub>O<sub>3</sub> (~90%) [42], Fe-Al-Ce oxide (95%) [51], and CaO nanoparticles (98%) [16].

## 4. Conclusions

PY, a food waste, was suggested as an adsorbent for fluoride removal, and its fluoride adsorption capacity was improved through thermal treatment. The mineral composition of PY changed from CaCO<sub>3</sub> to Ca(OH)<sub>2</sub> by thermal treatment, and the C content of PY was reduced by the liberation of CO<sub>2</sub> from PY. PY thermally treated at 800°C (PY-800) had a superior fluoride adsorption capacity than the other treated PYs. Fluoride removal by PY-800 was achieved through the formation of CaF<sub>2</sub> by reacting F<sup>-</sup> in the fluoride solution and Ca<sup>2+</sup> eluted from the adsorbent. Both the PFO and PSO models described the kinetic adsorption data well. Fluoride was adsorbed onto the surface of PY-800, which was revealed by the higher *R*<sup>2</sup> of the Langmuir model for the equilibrium isotherm data than that of the Freundlich model. The fluoride adsorption capacity of PY-800 was 159.62 mg/g, which is superior to that of other adsorbents reported in the literature and comparable to that of nano-sized adsorbents. Fluoride adsorption by PY-800 was an endothermic process and unspontaneous at 15°C–35°C. Fluoride adsorption by PY-800 was reduced by the increase in pH due to electrostatic repulsion and higher competition with OH<sup>-</sup> at higher pH. Bicarbonate, sulfate, and phosphate were inhibitors of fluoride for the adsorption to PY-800 as they also form precipitates with Ca<sup>2+</sup> ions. In conclusion, PY-800 is a suitable candidate for fluoride removal adsorbents owing to its low cost and high fluoride removal performance.

## Acknowledgement

This work was supported by the National Research Foundation of Korea (NRF) grant funded by the Korea government (MSIT) (No. 2020R1C1C1008982).

## References

- [1] M. Mohapatra, S. Anand, B.K. Mishra, D.E. Giles, P. Singh, Review of fluoride removal from drinking water, *J. Environ. Manage.*, 91 (2009) 67–77.
- [2] P.T. Harrison, Fluoride in water: a UK perspective, *J. Fluorine Chem.*, 126 (2005) 1448–1456.
- [3] K. Brinda, L. Elango, In: S.D. Monroy, Eds., *Fluoride: Properties, Applications and Environmental Management*, Nova Science Publishers, India, 2011, pp. 111–136.
- [4] WHO, *Guidelines for Drinking-Water Quality*, World Health Organization, Geneva, 1993.

- [5] K.K. Yadav, N. Gupta, V. Kumar, S.A. Khan, A. Kumar, A review of emerging adsorbents and current demand for defluoridation of water: bright future in water sustainability, *Environ. Int.*, 111 (2018) 80–108.
- [6] S. Ayoob, A.K. Gupta, V.T. Bhat, A conceptual overview on sustainable technologies for the defluoridation of drinking water, *Crit. Rev. Env. Sci. Technol.*, 38 (2008) 401–470.
- [7] A. Bhatnagar, E. Kumar, M. Sillanpää, Fluoride removal from water by adsorption—a review, *Chem. Eng. J.*, 171 (2011) 811–840.
- [8] P. Miretzky, A.F. Cirelli, Fluoride removal from water by chitosan derivatives and composites: a review, *J. Fluorine Chem.*, 132 (2011) 231–240.
- [9] A. Vinati, B. Mahanty, S.K. Behenra, Clay and clay minerals for fluoride removal from water: a state-of-the-art review, *Appl. Clay Sci.*, 114 (2015) 340–348.
- [10] M.J. Kim, S.H. Hong, J.I. Lee, C.G. Lee, S.J. Park, Removal of fluoride from water using thermally treated dolomite and optimization of experimental conditions using response surface methodology, *Desal. Water Treat.*, 155 (2019) 311–320.
- [11] J.-I. Lee, S.-H. Hong, C.-G. Lee, S.-J. Park, Experimental and model study for fluoride removal by thermally activated sepiolite, *Chemosphere*, 241 (2020) 125094, doi: 10.1016/j.chemosphere.2019.125094.
- [12] Y. Cengeloglu, E. Kir, M. Ersoz, Removal of fluoride from aqueous solution by using red mud, *Sep. Purif. Technol.*, 28 (2002) 81–86.
- [13] A. Blanco-Flores, N. Arteaga-Larios, V. Pérez-García, J. Martínez-Gutiérrez, M. Ojeda-Escamilla, I. Rodríguez-Torres, Efficient fluoride removal using Al-Cu oxide nanoparticles supported on steel slag industrial waste solid, *Environ. Sci. Pollut. Res.*, 25 (2018) 6414–6428.
- [14] B.W. Gu, C.G. Lee, S.J. Park, Application of response surface methodology and semi-mechanistic model to optimize fluoride removal using crushed concrete in a fixed-bed column, *Environ. Technol.*, 39 (2018) 616–627.
- [15] J.I. Lee, S.H. Hong, C.G. Lee, S.J. Park, Fluoride removal by thermally treated egg shells with high adsorption capacity, low cost, and easy acquisition, *Environ. Sci. Pollut. Res.*, 28 (2021) 35887–35901.
- [16] X. Wu, Y. Zhang, X. Dou, M. Yang, Fluoride removal performance of a novel Fe-Al-Ce trimetal oxide adsorbent, *Chemosphere*, 69 (2007) 1758–1764.
- [17] T. Poursaberi, M. Hassanisadi, K. Torkestani, M. Zare, Development of zirconium(IV)-metalloporphyrin grafted Fe<sub>3</sub>O<sub>4</sub> nanoparticles for efficient fluoride removal, *Chem. Eng. J.*, 189 (2012) 117–125.
- [18] V. Meilani, J.I. Lee, J.K. Kang, C.G. Lee, S. Jeong, S.J. Park, Application of aluminum-modified food waste biochar as adsorbent of fluoride in aqueous solutions and optimization of production using response surface methodology, *Microporous Mesoporous Mater.*, 312 (2021) 110764, doi: 10.1016/j.micromeso.2020.110764.
- [19] C. Shen, L. Wu, Y. Chen, S. Li, S. Rashid, Y. Gao, J. Liu, Efficient removal of fluoride from drinking water using well-dispersed monetite bundles inlaid in chitosan beads, *Chem. Eng. J.*, 303 (2016) 391–400.
- [20] J.I. Lee, J.K. Kang, S.H. Hong, C.G. Lee, S. Jeong, S.J. Park, Thermally treated *Mytilus coruscus* shells for fluoride removal and their adsorption mechanism, *Chemosphere*, 263 (2021) 128328, doi: 10.1016/j.chemosphere.2020.128328.
- [21] S.H. Yeom, K.Y. Jung, Recycling wasted scallop shell as an adsorbent for the removal of phosphate, *J. Ind. Eng. Chem.*, 15 (2009) 40–44.
- [22] N. Chen, W. Hu, C. Feng, Z. Zhang, Removal of phosphorus from water using scallop shell synthesized ceramic biomaterials, *Environ. Earth Sci.*, 71 (2014) 2133–2142.
- [23] T. Kanno, J.I. Horiuchi, Simultaneous removal behavior of phosphate and fluoride ions in the presence of scallop shell, *J. Chem. Eng. Jpn.*, 48 (2015) 276–280.
- [24] M. Ahmad, D.H. Moon, K.J. Lim, C.L. Shope, S.S. Lee, A.R. Usman, K.R. Kim, J.H. Park, S.O. Hur, J.E. Yang, Y.S. Ok, An assessment of the utilization of waste resources for the immobilization of Pb and Cu in the soil from a Korean military shooting range, *Environ. Earth Sci.*, 67 (2012) 1023–1031.
- [25] A. Abeynaike, L. Wang, M.I. Jones, D.A. Patterson, Pyrolysed powdered mussel shells for eutrophication control: effect of particle size and powder concentration on the mechanism and extent of phosphate removal, *Asia-Pac. J. Chem. Eng.*, 6 (2011) 231–243.
- [26] S. Hu, Y. Wang, H. Han, Utilization of waste freshwater mussel shell as an economic catalyst for biodiesel production, *Biomass Bioenergy*, 35 (2011) 3627–3635.
- [27] X. Fan, D.J. Parker, M.D. Smith, Adsorption kinetics of fluoride on low cost materials, *Water Res.*, 37 (2003) 4929–4937.
- [28] B.D. Turner, P. Binning, S.L.S. Stipp, Fluoride removal by calcite: evidence for fluorite precipitation and surface adsorption, *Environ. Sci. Technol.*, 39 (2005) 9561–9568.
- [29] K. Sasaki, M. Yoshida, B. Ahmmad, N. Fukumoto, T. Hirajima, Sorption of fluoride on partially calcined dolomite, *Colloids Surf., A*, 435 (2013) 56–62.
- [30] G.J. Chen, C.Y. Peng, J.Y. Fang, Y.Y. Dong, X.H. Zhu, H.M. Cai, Biosorption of fluoride from drinking water using spent mushroom compost biochar coated with aluminum hydroxide, *Desal. Water Treat.*, 57 (2016) 12385–12395.
- [31] J. Zhang, N. Chen, P. Su, M. Li, C. Feng, Fluoride removal from aqueous solution by zirconium-chitosan/graphene oxide membrane, *React. Funct. Polym.*, 114 (2007) 127–135.
- [32] C. Dwivedi, S.K. Pathak, M. Kumar, S.C. Tripathi, P.N. Bajaj, Preparation and characterization of potassium nickel hexacyanoferrate-loaded hydrogel beads for the removal of cesium ions, *Environ. Sci. Water Res.*, 1 (2015) 153–160.
- [33] H. Javed, D.X. Luong, C.G. Lee, D. Zhang, J.M. Tour, P.J. Alvarez, Efficient removal of bisphenol-A by ultra-high surface area porous activated carbon derived from asphalt, *Carbon*, 140 (2018) 441–448.
- [34] E. Bulet, M. Ozacar, I.A. Sengil, Adsorption of malachite green onto bentonite: equilibrium and kinetic studies and process design, *Microporous Mesoporous Mater.*, 115 (2008) 234–246.
- [35] G. Patel, U. Pal, S. Menon, Removal of fluoride from aqueous solution by CaO nanoparticles, *Sep. Sci. Technol.*, 44 (2009) 2806–2826.
- [36] S. Summers, D.R. Knappe, V.L. Snoeyink, In: J. Edzwald, Ed., *Water Quality and Treatment a Handbook on Drinking Water*, American Water Works Association, New York, 2011.
- [37] E. Tchongui-Kamaga, V. Alonzo, C.P. Nansou-Njiki, N. Audebrand, E. Ngameni, A. Darchen, Preparation and characterization of characterization of charcoals that the contain dispersed aluminum oxide as adsorbents for removal of fluoride from drinking water, *Carbon*, 48 (2010) 333–343.
- [38] S.S. Tripathy, J.L. Bersillon, K. Gopal, Removal of fluoride from drinking water by adsorption onto alum-impregnated activated alumina, *Sep. Purif. Technol.*, 50 (2006) 310–317.
- [39] J. Zhou, W. Zhu, J. Yu, H. Zhang, Y. Zhang, X. Lin, X. Luo, Highly selective and efficient removal of fluoride from ground water by layered Al-Zr-La Tri-metal hydroxide, *Appl. Surf. Sci.*, 435 (2018) 920–927.
- [40] S. Jain, R.V. Jayaram, Removal of fluoride from contaminated drinking water using unmodified and aluminum hydroxide impregnated blue lime stone waste, *Sep. Sci. Technol.*, 44 (2009) 1436–1451.
- [41] L.M. Camacho, A. Torres, D. Saha, S. Deng, Adsorption equilibrium and kinetics of fluoride on sol-gel-derived activated alumina adsorbents, *J. Colloid Interface Sci.*, 349 (2010) 307–313.
- [42] D. Dayanada, V.R. Sarva, S.V. Prasad, J. Arunachalam, N.N. Ghosh, Preparation of CaO loaded mesoporous Al<sub>2</sub>O<sub>3</sub>: Efficient adsorbent for fluoride removal from water, *Chem. Eng. J.*, 246 (2014) 430–439.
- [43] H. Hu, L. Yang, Z. Lin, X. Xiang, X. Jiang, L. Hou, Preparation and characterization of novel magnetic Fe<sub>3</sub>O<sub>4</sub>/chitosan/Al(OH)<sub>3</sub> beads and its adsorption for fluoride, *Int. J. Biol. Macromol.*, 114 (2018) 256–262.
- [44] V. Gopalakannan, S. Periyasmy, N. Viswanathan, Fabrication of magnetic particles reinforced nano-hydroxyapatite/gelatin composite for selective Cr(VI) removal from water, *Environ. Sci. Water Recur.*, 4 (2018) 783–794.

- [45] S. Shahabuddin, C. Tashakori, M.A. Kamboh, Z.S. Korrani, R. Saidur, H.R. Nodeh, M.E. Bidhendi, Kinetic and equilibrium adsorption of lead from water using magnetic metformin-substituted SBA-15, *Environ. Sci. Water Res.*, 4 (2018) 549–558.
- [46] J. Ma, Y. Shen, Y. Shen, Y. Wen, W. Liu, Al-doping chitosan-Fe(III) hydrogel for the removal of fluoride from aqueous solutions, *Chem. Eng. J.*, 248 (2014) 98–106.
- [47] Y. Tang, X. Guan, J. Wang, N. Gao, M.R. McPhail, C.C. Chusuei, Fluoride adsorption onto granular ferric hydroxide: effects of ionic strength, pH, surface loading, and major co-existing anions, *J. Hazard. Mater.*, 171 (2009) 774–779.
- [48] M.G. Sujana, G. Soma, N. Vasumathi, S. Anand, Studies on fluoride adsorption capacities of amorphous Fe/Al mixed hydroxide from aqueous solutions, *J. Fluorine Chem.*, 130 (2009) 749–754.
- [49] X. Dou, D. Mohan, C.U. Pittman Jr., S. Yang, Removing fluoride from water using hydrous zirconium oxide, *Chem. Eng. J.*, 198 (2012) 236–245.
- [50] J. Wang, X. Lin, X. Luo, Y. Long, A sorbent of carboxymethyl cellulose loaded with zirconium for the removal of fluoride from aqueous solution, *Chem. Eng. J.*, 252 (2014) 415–422.
- [51] E. Oguz, Adsorption of fluoride on gas concrete material, *J. Hazard. Mater.*, 117 (2005) 227–233.